

Fast-response liquid-crystal displays using crossed fringe fields

Yan Li (SID Student Member)

Zhibing Ge (SID Member)

Ruibo Lu (SID Member)

Meizi Jiao (SID Student Member)

Shin-Tson Wu (SID Fellow)

Abstract — A fast-response and wide-view liquid-crystal display (LCD) using the crossed fringe-field-switching (CFFS) mode is proposed, where the fringe-field electrodes exist on both the top and bottom substrates. The bottom fringe field is used to turn on the LC directors and the top fringe field is used to assist in the LC decay process. The decay time is reduced by $\sim 2\times$ compared to that of the conventional FFS mode between the full bright and dark states, and more than a $2\times$ improvement is obtained for other gray-scale transitions. This CFFS mode also preserves the wide-view characteristics as the conventional FFS mode. Its applications to LCD TVs and monitors for reducing image blur are addressed.

Keywords — *Liquid-crystal display, crossed electric fields, fast response time.*

DOI # 10.1889/JSID16.10.1069

1 Introduction

In-plane switching (IPS)¹ and fringe-field-switching (FFS)^{2,3} liquid-crystal displays (LCDs) exhibit wide view and a weak color shift due to the in-plane LC reorientations. Because of the large aperture ratio, the overall transmittance of an FFS LCD is comparable to that of a twisted-nematic (TN) panel⁴; however, its response time still remains a challenge. For video applications, a response time as fast as 3 msec is usually required in order to minimize the image blur of moving images. The response time of a LC device is mainly governed by the cell gap, viscoelastic coefficient, anchoring energy, biased voltage, and applied voltage.⁵ Several approaches have been proposed to improve response time, such as overdrive and undershoot voltage method,^{6,7} crossed-field method,^{8–11} thin cell method,^{12–14} and bend cell.^{15–18} Among the abovementioned approaches, thin cells with overdrive and undershoot voltages and bend cells have been widely employed in LCD TVs.

To further improve response time, the crossed-field method, which was first demonstrated more than three decades ago,^{8,9} has received renewed interest. More recently, Xiang *et al.* proposed the use of double FFS electrodes¹¹ to improve LC response time. In this approach, both of the FFS electrodes are set perpendicular to each other on both the bottom and top substrates. The LC cell under a bright state is switched by the fringe fields generated from both substrates, making the cell functions like two cascaded half-cells. During the LC decay process, voltages on both electrodes are removed to let the two effective half-cells relax independently. As a result, fast response time can be achieved.

In this paper, we propose a crossed fringe-field-switching (CFFS) method to improve the response time of an LCD with homogeneous alignment, based on a different mechanism. The FFS electrodes are formed on both substrates, where the LC cell is only driven by the bottom electrodes to achieve different gray levels, and the top FFS electrodes are merely used to accelerate the switch-off process. In order to lower the required voltage burst, the elec-

trodes of the bottom and top substrates are set at 60° . Applying a 10-V voltage to the top electrodes, we obtained $\sim 2\times$ improvement in the turn-off time. In addition, this device also exhibits a wide viewing angle, similar to the conventional FFS mode.

2 Device structure and operating mechanism

Figure 1(a) illustrates a cross-sectional view of the CFFS device structure and Fig. 1(b) shows the top view of the top and bottom electrodes. On both top and bottom substrates, strip pixel electrodes and planar ITO (indium tin oxide) common electrodes are formed with a SiO_2 passivation layer (200 nm thick) in between. The bottom strip electrodes are perpendicular, while the top strip electrodes are at an angle α to the x axis. The LC cell has an initial homogeneous alignment and the employed LC has a negative dielectric anisotropy ($\Delta\epsilon < 0$). The bottom FFS electrodes are used to drive the LC cell to different gray levels and the top electrodes are used to accelerate the LC decay process. To lower the driving voltage, the rubbing direction of the LC cell is set at about 10° with respect to the x axis, *i.e.*, 80° between the LC axis and the electrode stripes. The LC cell is further interposed between two crossed linear polarizers with the LC rubbing direction parallel to the bottom polarizer's transmission axis.

In the null-voltage state, the light passing the bottom polarizer keeps its polarization state when traversing through the LC layer and is blocked by the top linear polarizer, resulting in a dark state. For a bright state, a driving voltage is only applied to the bottom pixel electrode, while the top electrodes are grounded. Thus, fringe fields with rich horizontal components are generated near the bottom substrate, which reorient the LC directors in the counterclockwise direction causing light transmission. During decay period, the voltage of the bottom pixel electrode is released and a pulse voltage is applied to the top pixel electrode. The fringe fields from the top substrate push the LC molecules to decay quickly toward their initial states. Here, the align-

The authors are with the University of Central Florida, College of Optics and Photonics, 4000 Central Florida Blvd., Orlando, FL 32816-2700 USA; telephone 407/823-4763, fax -6880, e-mail: swu@mail.ucf.edu.

© Copyright 2008 Society for Information Display 1071-0922/08/1610-1069\$1.00

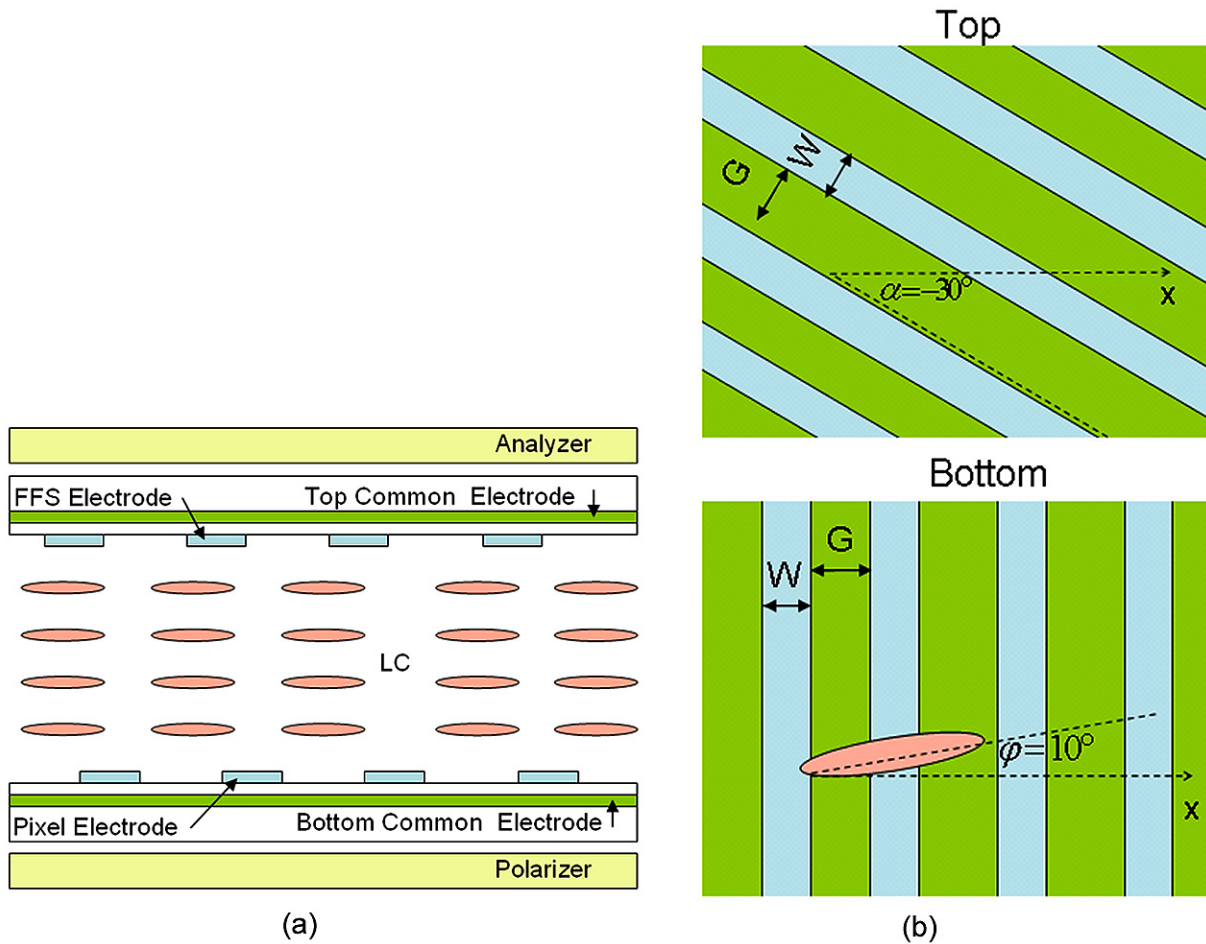


FIGURE 1 — (a) Cross-sectional view and (b) top view of the CFFS cell.

ment angle of the top pixel electrode is critical for this acceleration process. In the full bright state, the LC directors are reoriented at $\sim 40^\circ\text{--}50^\circ$ from their initial axis by the bottom fringe fields.³ Thus, we intentionally set the top electrodes to be about -30° from the x axis. Under such a circumstance, the top electrode stripes are also at $\sim 80^\circ$ to the effective on-state LC orientation axis in order to lower the required erasing pulse voltage.

3 Simulation results

To validate our approach, we employed the commercial 3D LC simulator TECH-WIZ (from Sanayi Company) to calculate the electro-optic properties of our design. The width and gap of the pixel electrodes are set at $W = 3\ \mu\text{m}$ and $G = 4\ \mu\text{m}$, respectively, on both substrates. The LC cell and material parameters are listed as follows: cell gap, $3\ \mu\text{m}$; birefringence, $\Delta n = 0.11$ at $\lambda = 550\ \text{nm}$; dielectric anisotropy, $\Delta\epsilon = -4.0$; elastic constants, $K_{11} = 13.5\ \text{pN}$, $K_{22} = 7.0\ \text{pN}$, and $K_{33} = 15.1\ \text{pN}$; and rotational viscosity $\gamma_1 = 136\ \text{mPa}\cdot\text{sec}$. As a reference, we also simulated a conventional FFS cell using the same parameters and material, except that the electrodes are only formed on the bottom substrate.

The performances of these two structures are simulated using 2×2 extended Jones matrices.^{19,20}

3.1 VT curves

The voltage-dependent transmittance (V - T) curves of the conventional FFS cell and the CFFS cell are shown in Fig. 2. The conventional FFS mode has a threshold voltage at $1.0\ V_{\text{rms}}$. Its transmittance reaches 10% of maximum at $V \sim 2.2\ V_{\text{rms}}$, 50% at $\sim 3.1\ V_{\text{rms}}$, and 100% at $\sim 6.0\ V_{\text{rms}}$. The maximum transmittance of the FFS cell sandwiched between two crossed polarizers is $\sim 35\%$, compared to 37.5% for two parallel linear polarizers alone. By contrast, the threshold voltage of the CFFS cell is also about $1.0\ V_{\text{rms}}$, but its on-state voltage is increased to $8\ V_{\text{rms}}$ and the maximum transmittance decreased to 32%. Its 10% and 50% transmittance occurs at $V \sim 2.2\ V_{\text{rms}}$ and $3.4\ V_{\text{rms}}$, respectively. Based on these comparisons, our CFFS structure shows a slightly lower transmittance and higher on-state voltage. This is because the grounded electrodes weaken the fringe fields near the top substrate, and thus the LCs do not rotate as much as in a conventional FFS cell. However, as described in the following section, the top fringing field would improve LC relaxation time by $\sim 2\times$.

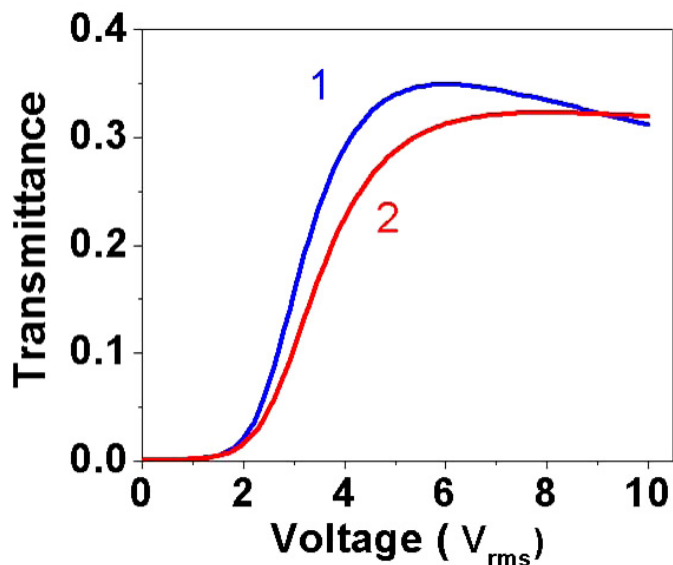


FIGURE 2 — Voltage-dependent transmittance curves. Curve 1 is for the FFS cell and curve 2 is for the CFFS cell.

3.2 Driving schemes and response times between different gray levels

Figure 3(a) shows the driving scheme of the pixel electrode for the conventional FFS cell switching from an initial gray level V_i to a final gray level V_f . And Fig. 3(b) illustrates the undershoot method where the voltage is first switched off for a short period (until the transmittance decays to the designated gray level) and then followed by a bias voltage to hold the transmittance at the targeted final gray level V_f . Due to this undershoot voltage, a faster response time can be achieved. On the other hand, the CFFS mode utilizes a different scheme as shown in Fig. 3(c) to achieve an even faster decay time. When the cell is driven to a gray level (V_i) by the bottom electrodes, the top pixel electrodes are kept at $0 V_{rms}$. As the relaxation process begins, the bottom pixel voltage is switched off, while a short pulse voltage is instantly applied to the top pixel electrode to expedite the LC decay process. In addition to the natural decay originating from the elastic torque, during this short period, fringe fields from the top substrates help to push the LCs to their targeted states. After a proper time T_1 , the pulse voltage is removed and the cell undergoes a natural decay again for another short period T_2 . The purpose of this additional short undershoot will be explained later. When the transmittance level is close to the desired final state, the driving pixel electrode on the bottom substrate is then biased back to the targeted gray level V_f .

We also studied the dynamic response for different gray-to-gray transitions at $T = 100\%$, 50% , 10% , and 0% to validate this concept. With the assistance of this extra pushing electric fields, our new design exhibits an $\sim 2\times$ faster decay time than the conventional FFS cell using the undershoot method alone, and the improvement for gray-to-gray transitions is even more pronounced if compared to a conventional FFS cell with a natural decay process.

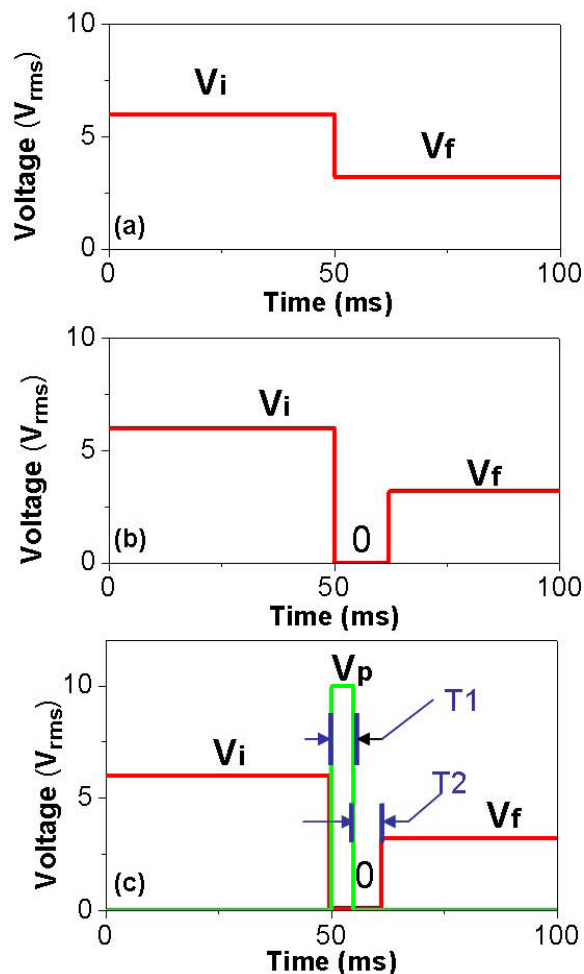


FIGURE 3 — (a) Conventional voltage driving scheme for a gray-to-gray level transition, (b) undershoot driving scheme, and (c) new driving scheme for the CFFS cell.

Figure 4 shows the decay time for the 100% to 0% transition. For the FFS mode studied, its decay time is ~ 23.3 msec (based on 90–10% transmittance change). But

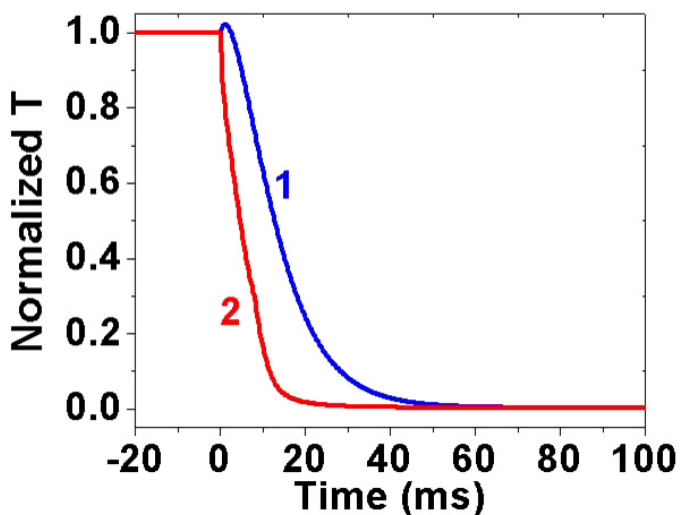


FIGURE 4 — Decay times for the transmittance change from 100% to 0%. Curve 1 is for the FFS structure and curve 2 is for the CFFS structure with $T_1 = 8$ msec.

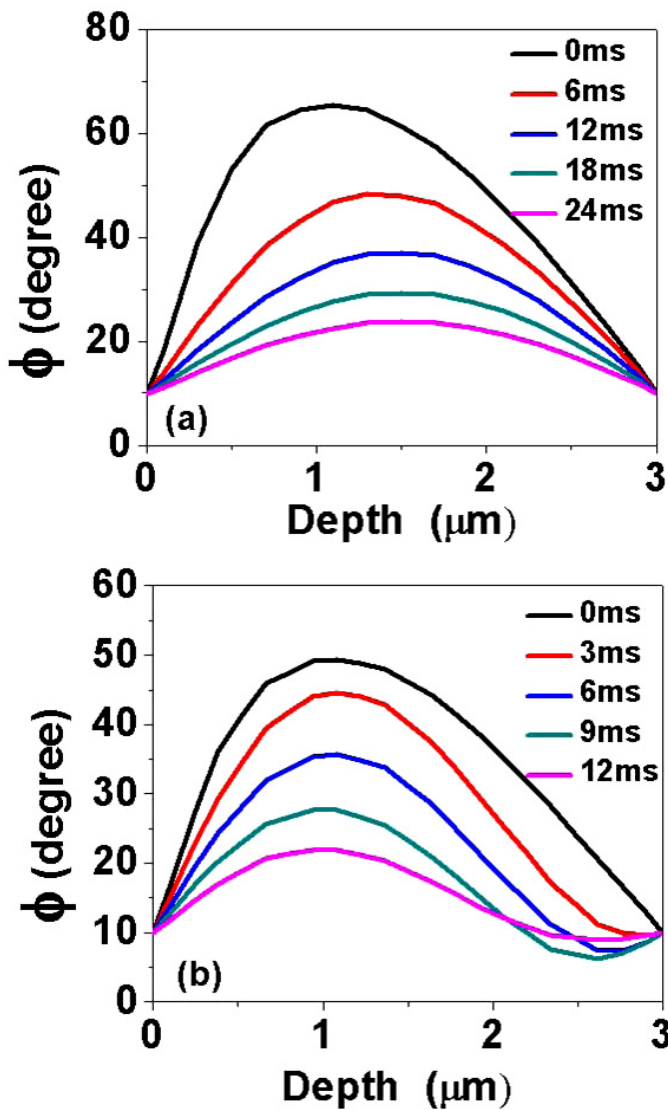


FIGURE 5 — LC azimuthal angle distributions for (a) FFS mode at every 6 msec after the decay process starts and (b) CFFS mode at every 3 msec after the decay process has started.

for the CFFS structure, when the duration of the pushing pulse is $T_1 \sim 8$ msec and the pulse voltage ~ 10 V_{rms}, we obtain an overall decay time of ~ 11.1 msec. The improvement is $\sim 2\times$. To understand this difference, we compare the LC directors' distribution of the two cells.

Figures 5(a) and 5(b) show the LC directors distribution of a conventional FFS and CFFS mode, respectively. In the FFS mode, LC directors gradually relax to their initial positions after the applied voltage is removed instantaneously. But this process is relatively slow because it is governed by the elastic restoring force of the LC cell. On the other hand, in the CFFS mode, the pushing fields from the top FFS electrodes help to expedite the LC relaxation towards their initial alignment, in addition to the restoring elastic torque. However, the pushing fringe fields are mainly confined near the top substrate, thus the liquid crystals near the top substrate are slightly over-rotated at the very beginning. After the pushing voltage on the top electrodes is removed at $t = 8$ msec (when the gray level is close to its

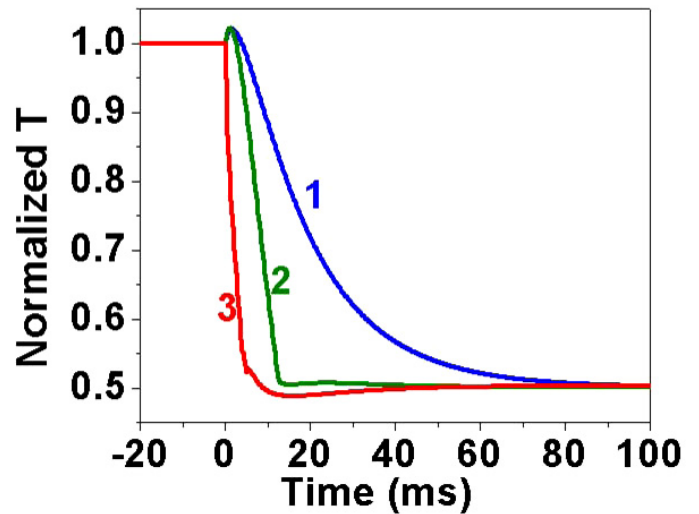


FIGURE 6 — Decay times for the gray-scale transition from 100% to 50%. Curve 1 is for the FFS structure, curve 2 is for the FFS with undershoot, and curve 3 is for the CFFS structure with $T_1 = 4$ msec and $T_2 = 1$ msec.

targeted value), both bottom and top LCs can be pulled back by the surface anchoring quickly. From this LC director plot, we find that the voltage bursting time also plays a very critical role: a longer time will over-rotate the LC directors which, in turn, results in a slow recovering time. From our studies, we found the pulsing time of ~ 8 msec is optimal. And for other gray-to-gray transitions, this pulsing time needs to be adjusted and can be stored in a look-up table.

Figure 6 shows the turn-off time for the 100% to 50% transition. For conventional FFS cell, the response time corresponding to the driving scheme of Fig. 3(a) is ~ 38.3 msec, while when using the undershoot driving scheme shown in Fig. 3(b), the response time is 7.7 msec. For the CFFS structure, when the duration of the pushing pulse is $T_1 = 4$ msec and the duration of the followed undershoot voltage is $T_2 = 1$ msec, we obtain a decay time of ~ 3.8 msec, which is only $\sim 50\%$ of that for the conventional FFS cell using the undershoot method, and only $\sim 10\%$ of the natural decay conventional cell. Here, the 1 msec additional duration of the undershoot voltage is required because the top-half LCs are also slightly over-twisted by the fields there, as indicated in Fig. 5(b). The response time here is also defined as the time for the transmittance changes (between levels V_i and V_f) from 90% to 10%. Thus, it is slightly shorter than $T_1 + T_2$.

Similarly, the dynamic response from the 50% to 10% transition is shown in Fig. 7. For the conventional FFS mode without undershoot voltage, the response time is ~ 41.8 msec, while it is reduced to ~ 11.5 msec with undershoot. For the CFFS structure, we set the duration of the pulsing voltage at $T_1 = 2$ msec and undershoot at $T_2 = 3$ msec, the decay time is reduced to ~ 4.5 msec. The improvement is also $\sim 2\times$ of the undershoot method and $\sim 9\times$ of the natural decay process. From these analyses, we can see that it is possible to drive the FFS cell with an average gray-to-gray

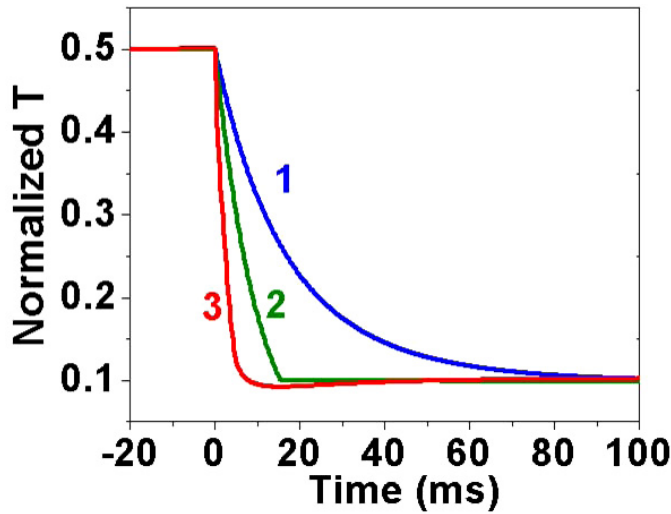


FIGURE 7 — Decay times for the gray-scale transition from 50% to 10%. Curve 1 is for the FFS cell, curve 2 is for the FFS cell with undershoot, and curve 3 is for the CFFS cell with $T_1 = 2$ msec and $T_2 = 3$ msec.

response time below 5 msec, which is highly preferred for video applications.

3.3 Viewing angle

Because the initial LC molecular distribution in the CFFS cell is identical to that of the conventional FFS mode, a similar viewing-angle performance is expected. Figure 8 shows the iso-contrast contour plot of the CFFS cell without using any compensation films. We can obtain a contrast ratio greater than 10:1 over the 60° viewing cone. By proper film compensation, it can be easily expanded to over 80° .²¹

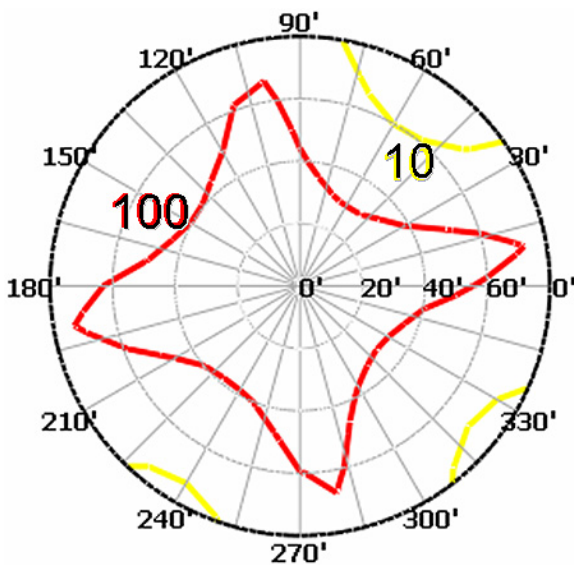


FIGURE 8 — Iso-contrast contour plot of the CFFS cell without using any compensation films.

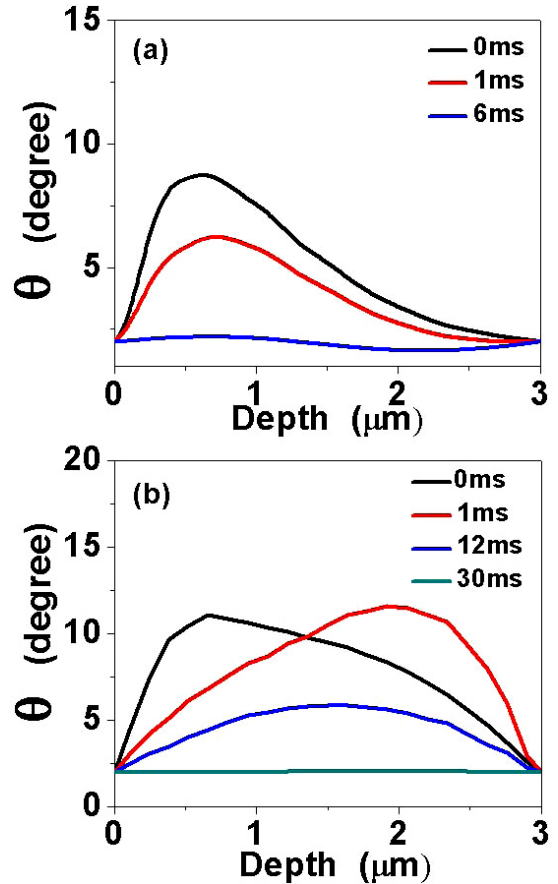


FIGURE 9 — Simulated LC tilt angle distributions for (a) FFS mode and (b) CFFS mode at different time stages after the decay process has started.

4 Discussion

As noted in Figs. 4 and 6, there is an optical bounce in the beginning of the switch-off process for the FFS cell, but not in the CFFS cell. To explain these phenomena, we have calculated the transient tilt-angle distribution of the two LC cells. Figures 9(a) and 9(b) show the tilt angle (θ) distribution of the FFS and CFFS modes, respectively. For the FFS mode, the LC directors near the pixel electrode edges (depth, $\sim 0.5 \mu\text{m}$) have a small tilt angle (about 8°) along the vertical direction in addition to the azimuthal rotation in a bright state. When the voltage is released, the LC directors there would both tilt down (governed by K_{33}) and rotate in plane (governed by K_{22}). Because K_{33} is larger than K_{22} , the tilt down is faster than the horizontal rotation. As a result, the overall effective phase change $d(n_{\text{eff}} - n_o)/\lambda$ will increase first (because n_{eff} becomes larger), exhibiting an increased transmittance (optical bounce) at first. As the reduction of phase change is later governed by the in-plane rotation of LCs, the transmittance then keeps decreasing.

For the CFFS mode, the LC directors in the gray-level transitions experience a different reorientation process. As shown in Fig. 9(b), strong fringe fields are introduced from the top electrodes immediately after the transition starts, causing the LC directors near the top substrate to have a large tilt angle at the very beginning. Conse-

quently, in addition to the in-plane LC rotation, the effective phase change continues to decrease and a monotonous reduction of transmittance is observed.

5 Conclusion

We demonstrated a crossed FFS structure to improve the turn-off time. By using a pulse voltage on the top pixel electrodes, the LC molecules are expedited to decay back to their initial alignment direction. By proper cell configuration and driving schemes, we are able to reduce the response time by $\sim 2\times$ as compared to a conventional FFS cell even when using the undershoot method. We also examine its iso-contrast plot and prove that it also has a wide view angle. Two tradeoffs are found: the on-state voltage is increased and the maximum transmittance is slightly decreased.

Acknowledgments

The authors are indebted to Chi-Mei Optoelectronics for the financial support.

References

- 1 M. Oh-e and K. Kondo, *Appl. Phys. Lett.* **67**, 3895 (1995).
- 2 S. H. Lee, S. L. Lee, and H. Y. Kim, *Appl. Phys. Lett.* **73**, 2881 (1998).
- 3 Z. Ge, S. T. Wu, S. S. Kim, J. W. Park, and S. H. Lee, *Appl. Phys. Lett.* **92**, 181109 (2008).
- 4 M. Schadt and W. Helfrich, *Appl. Phys. Lett.* **18**, 127 (1971).
- 5 S. T. Wu and D. K. Yang, *Reflective Liquid Crystal Displays* (Wiley, New York, 2001).
- 6 S. T. Wu and C. S. Wu, *J. Appl. Phys.* **65**, 527 (1989).
- 7 S. T. Wu, *Appl. Phys. Lett.* **57**, 986 (1990).
- 8 D. J. Channin, *Appl. Phys. Lett.* **26**, 603 (1975).
- 9 D. J. Channin and D. E. Carlson, *Appl. Phys. Lett.* **28**, 300 (1976).
- 10 S. T. Wu, *J. Appl. Phys.* **58**, 1419 (1985).
- 11 C. Y. Xiang, X. Y. Sun, and X. J. Yin, *Appl. Phys. Lett.* **83**, 5154 (2003).
- 12 S. T. Wu and U. Efron, *Appl. Phys. Lett.* **48**, 624 (1986).
- 13 S. Gauza, X. Zhu, S. T. Wu, W. Piecsek, and R. Dabrowski, *J. Display Technol.* **3**, 250 (2007).
- 14 M. Jiao, Z. Ge, Q. Song, and S. T. Wu, *Appl. Phys. Lett.* **92**, 061102 (2008).
- 15 P. J. Bos and K. R. Koehler/Beran, *Mol. Cryst. Liq. Cryst.* **113**, 329 (1984).
- 16 T. Miyashita, Y. Yamaguchi, and T. Uchida, *Jpn. J. Appl. Phys. Part 2*, **34**, L177 (1995).
- 17 F. S. Yeung, Y. W. Li, and H. S. Kwok, *Appl. Phys. Lett.* **88**, 041108 (2006).
- 18 M. Jiao, Z. Ge, S. T. Wu, and W. K. Choi, *Appl. Phys. Lett.* **92**, 111101 (2008).
- 19 A. Lien, *Appl. Phys. Lett.* **57**, 2767 (1990).
- 20 Z. Ge, T. X. Wu, X. Zhu, and S. T. Wu, *J. Opt. Soc. Am. A* **22**, 966 (2005).
- 21 X. Zhu, Z. Ge, and S. T. Wu, *J. Display Technol.* **2**, 2 (2006).